Research Square

Preprints are preliminary reports that have not undergone peer review.
They should not be considered conclusive, used to inform clinical practice,
or referenced by the media as validated information.

An anesthesia-related gene signature is associated with prognosis and immune phenotypes in colorectal cancer: a retrospective multi-cohort bioinformatics study

Yu Zhang
Gaoyang County Hospital
Wangyang Zhang
Gaoyang County Hospital
Meng Sha
Gaoyang County Hospital
Qiang Wang
Gaoyang County Hospital
Weixian Xie
2026691021@gzhmu.edu.cn

Affiliated Qingyuan Hospital,Guangzhou Medical University,Qingyuan People's Hospital

Research Article

Keywords: Colorectal cancer, Anesthesia-related genes, Prognostic signature, Tumor immune microenvironment, Immune-response proxies, LASSO Cox regression

Posted Date: October 21st, 2026

DOI: https://doi.org/10.21203/rs.3.rs-11130997/v1

License: This work is licensed under a Creative Commons Attribution 4.0 International License.
Read Full License

Additional Declarations: No competing interests reported.

Abstract

Background

Emerging evidence suggests that anesthetic agents are associated with cancer recurrence, yet the molecular pathways linking anesthesia and colorectal cancer (CRC) progression remain unclear. This study constructed a prognostic signature based on anesthesia-related genes (ARGs) and evaluated associations with inferred immune phenotypes in CRC.

Methods

ARGs were compiled from a transcriptomic dataset comparing propofol and sevoflurane anesthesia (GSE179004) and a systematic literature review. Differentially expressed ARGs were identified in TCGA-CRC (649 tumors, 51 normal tissues) using DESeq2. A LASSO Cox model was trained on TCGA and evaluated in two GEO cohorts (GSE17536, GSE39582). Immune infiltration was assessed by CIBERSORT and ESTIMATE; immunotherapy-response proxies by TIDE and Immunophenoscore frameworks; pathway and drug-sensitivity hypotheses by GSEA and oncoPredict.

Results

Seventy-eight differentially expressed ARGs were identified. A 15-gene signature showed moderate discrimination in TCGA (C-index 0.682) and GSE17536 (0.668–0.681) but weak transportability to GSE39582 (0.535). The risk score remained associated with outcome after clinical adjustment (HR 2.27, 95% CI 1.51–3.43). High-risk tumors showed higher inferred M2 macrophage and regulatory T-cell scores and less favorable TIDE/IPS classifications. GSEA, in silico drug-sensitivity, and Human Protein Atlas analyses generated pathway and corroboration hypotheses.

Conclusions

The signature was associated with prognosis and inferred immune phenotypes in the development cohort and one external cohort, but performance approached chance in GSE39582. TIDE, IPS, drug-sensitivity, and protein-atlas findings represent computational corroboration rather than experimental validation; cross-platform recalibration and independent validation are required before clinical interpretation.

Trial registration

Not applicable. This study is a retrospective, multi-cohort bioinformatics analysis of publicly available, de-identified datasets and is not a clinical trial; no prospective recruitment, intervention, or new human

data collection was involved.

Introduction

Colorectal cancer (CRC) is one of the most common gastrointestinal malignancies worldwide, characterized by high postoperative recurrence and distant metastasis, which severely compromise the long-term survival of surgical patients. Surgical resection remains the primary curative treatment for localized CRC, and nearly all patients receive general anesthesia during perioperative management. Accumulating clinical and preclinical evidence has demonstrated that different anesthetic regimens, including intravenous propofol and inhaled sevoflurane, are differentially associated with tumor proliferation, epithelial–mesenchymal transition, cancer stem cell activity, and systemic antitumor immune function [1–3]. Nevertheless, clinical studies regarding the prognostic impact of anesthetic techniques on CRC patients remain inconsistent, and the underlying molecular mechanism by which perioperative anesthesia is associated with CRC progression has not been systematically elucidated.

Anesthetics are significantly associated with transcriptomic changes in colorectal tumor cells and the tumor microenvironment composition (TME) through modulation of specific downstream target genes. Genes differentially expressed in response to anesthetic stimulation are defined as anesthesia-related genes (ARGs), which are considered promising biomarkers for evaluating tumor malignant phenotypes and clinical prognosis [4, 5]. At present, most existing studies focus on single-gene functional exploration of anesthetic drugs, while comprehensive transcriptome research constructing prognostic signatures based on ARGs in CRC is still lacking. Reliable ARG-based risk stratification models are needed to identify high-risk CRC populations, clarify the molecular correlation between perioperative anesthesia and tumor prognosis, and guide individualized anesthetic and adjuvant therapeutic strategies.

Importantly, although the ARG catalog was initially derived from neural tissue transcriptomics, growing evidence demonstrates that neurotransmitter receptors—including GABA-A receptors, dopamine receptors, nicotinic acetylcholine receptors, and voltage-gated ion channels—are aberrantly expressed in colorectal and other epithelial cancers and play functional roles in tumor proliferation, migration, and immune modulation [5–9]. For example, GABA-A receptor subunits modulate CRC cell proliferation via the GABA-PI3K/AKT axis, dopamine signaling through D2-family receptors has been implicated in gastrointestinal tumor cell growth, and voltage-gated calcium channels are emerging therapeutic targets in CRC. These findings provide biological rationale for investigating anesthesia-responsive neural genes as prognostic markers in CRC, even though the original transcriptomic signatures were identified in neural tissue. The term "anesthesia-related genes" is used throughout this study to denote genes whose expression is associated with anesthetic pharmacological targets, without implying direct causal regulation of CRC by anesthetic agents.

In this study, we systematically curated anesthesia-responsive genes from published transcriptomic datasets and a systematic literature review. Transcriptomic and clinical data of CRC patients were

retrieved from The Cancer Genome Atlas (TCGA) as the training cohort, and multiple Gene Expression Omnibus (GEO) datasets were applied for external evaluation. Least absolute shrinkage and selection operator (LASSO) Cox regression analysis was performed to screen prognostic ARGs and construct a novel ARG-based prognostic signature. Subsequently, we systematically compared differences in clinical prognosis, tumor immune infiltration landscape, immune checkpoint molecule expression, tumor mutational burden (TMB), functional pathway enrichment, and chemotherapeutic drug sensitivity between high-risk and low-risk subgroups. Furthermore, we evaluated the capability of this signature to examine TIDE/IPS proxy scores related to immune checkpoint inhibitor (ICI) response.

Methods

Data acquisition and anesthesia-related gene collection

Transcriptomic expression data (STAR - Counts workflow) and corresponding clinical information of CRC patients, including colon adenocarcinoma (COAD) and rectal adenocarcinoma (READ), were downloaded from the TCGA database via the GDC API (https://api.gdc.cancer.gov). The dataset comprised 700 samples (649 tumors, 51 adjacent normal tissues) with 60,660 genes. Patients with incomplete survival information or zero survival time were excluded, yielding 590 patients with complete OS data for model construction. Two independent GEO datasets were enrolled as external cohorts: GSE39582 (585 samples, GPL570 platform) and GSE17536 (177 samples, GPL570 platform). Survival data for TCGA-CRC were obtained from UCSC Xena. All expression data were $\log_2$-transformed; TPM values were used for TCGA, and MAS5-normalized expression values were used for GEO datasets after probe-to-gene annotation using GPL570.

ARGs were compiled from two sources: (i) an exploratory six-sample microarray comparison of glioblastoma specimens exposed to propofol-remifentanil (n = 3) or sevoflurane-remifentanil (n = 3; GSE179004), using a nominal $P < 0.05$ and $|\log2 \text{ fold change}|>0.5$, and (ii) genes reported in a systematic literature review. The small discovery dataset and absence of false-discovery-rate control are important limitations; the resulting catalog was treated as hypothesis-generating. Acknowledging that Benjamini–Hochberg correction is mathematically conservative for n = 3 per group and 48,296 tested transcripts (minimum nominal $P = 8.04\times10^{-5}$ yielding minimum adjusted $P = 0.989$, with zero genes surviving FDR < 0.05), nominal-P screening was retained only for catalog construction; downstream survival modeling relied on the LASSO-penalized multivariate Cox procedure and was not influenced by the DEARG FDR threshold.

Identification of differentially expressed ARGs

Differential expression analysis between tumor and normal tissues in TCGA-CRC was performed using pyDESeq2 (Python implementation of DESeq2). Genes with fewer than 10 total counts across all samples were filtered out, leaving 54,437 genes for analysis. The thresholds for differentially expressed

genes (DEGs) were $|\log_2 FC| > 1$ and adjusted $P < 0.05$ (Benjamini–Hochberg correction). DEARGs were defined as the intersection of DEGs and the ARG catalog. KEGG and GO functional enrichment analyses of DEARGs were performed using Enrichr.

Development and evaluation of the ARG prognostic signature

For model development, the 78 DEARGs were filtered to 35 genes with measurable expression across the analyzed platforms. Univariate Cox screening followed by L1-penalized Cox regression with 10-fold cross-validation was used to derive a 15-gene model, and the risk score was calculated from the fitted gene coefficients. TCGA patients were divided at the median score for descriptive survival analyses. A secondary sensitivity analysis compared L1-penalized Cox regression with least-squares Lasso screening; only four genes overlapped and apparent training C-indices differed (0.696 versus 0.654). Because feature screening and performance assessment were conducted within the same development cohort and the two methods optimize different objectives, internal estimates may be optimistic and the sensitivity comparison is not evidence of model stability. All preprocessing, normalization, cross-validation folds, and coefficient fits used a fixed random seed (random_state = 42); training-feature selection (univariate Cox + LASSO) and model evaluation on TCGA were performed within the same development cohort but with the held-out external GEO cohorts providing the principal transportability assessment, mitigating information leakage between TCGA feature selection and TCGA C-index estimation.

Kaplan–Meier survival analysis with the log-rank test was used to compare survival differences between groups. The concordance index (C-index) was calculated to evaluate discriminative ability. For cross-platform evaluation, Z-score normalization and rank-based normalization were compared. In GSE17536, disease-free survival (DFS) and disease-specific survival (DSS) were used as endpoints. In GSE39582, relapse-free survival (RFS) was used.

Independent prognostic analysis and nomogram construction

Univariate and multivariate Cox regression analyses incorporating clinical characteristics (age, sex, TNM stage, T classification, N classification, M classification) and the risk score were performed to identify independent prognostic factors. Time-dependent receiver operating characteristic (ROC) curves at 1, 3, and 5 years were used to assess predictive accuracy. A predictive nomogram integrating independent prognostic factors was constructed. Calibration curves and decision curve analysis (DCA) were plotted to evaluate model calibration and clinical net benefit.

Tumor immune microenvironment analysis

CIBERSORT (Cell type Identification By Estimating Relative Subsets Of RNA Transcripts) deconvolution with the LM22 leukocyte signature matrix (1,000 permutations) was applied to quantify the abundance

of 22 immune cell types. The ESTIMATE algorithm was used to calculate immune scores, stromal scores, and ESTIMATE scores. Single-sample GSEA (ssGSEA) was additionally performed to compute infiltration scores for 22 immune cell types across all TCGA-CRC tumors. Spearman correlation analysis between each of the 15 model genes and ssGSEA-based immune cell scores was performed, with Benjamini–Hochberg FDR correction.

TMB and immune-response proxy analysis

Somatic mutation data for TCGA-COAD and TCGA-READ were obtained from the GDC Data Portal, and tumor mutational burden was calculated as nonsynonymous mutations per megabase. TIDE and IPS were computed as transcriptome-derived proxy scores. Their published response-associated thresholds were summarized descriptively; no observed immunotherapy response data were available in the analyzed cohorts.

Gene set enrichment analysis

GSEA was performed using gseapy with MSigDB Hallmark, KEGG, and Reactome gene set collections. Genes were ranked by signal-to-noise ratio between high- and low-risk groups. 1,000 permutations were used for significance testing. Pathways with FDR < 0.25 were considered nominally significant; FDR < 0.05 was considered strictly significant.

Drug sensitivity analysis

Drug sensitivity prediction was performed using a ridge regression approach trained on GDSC2 pharmacogenomic data (805 cell lines, 198 drugs). The GDSC2 expression matrix was used as the training set, and predicted IC_{50} values for 183 drugs (with sufficient valid cell lines) were computed for each TCGA-CRC patient. Differences in predicted IC_{50} between high- and low-risk groups were assessed using the Wilcoxon rank-sum test with Benjamini–Hochberg correction. This approach functionally recapitulates the oncoPredict algorithm (a ridge regression-based drug sensitivity prediction tool).

Protein-level corroboration using the Human Protein Atlas

Immunohistochemistry data for the 15 model genes in colorectal cancer tissue were retrieved from the Human Protein Atlas (HPA) database (https://www.proteinatlas.org). Protein expression intensity, subcellular localization, and prognostic marker annotations were recorded for each gene.

Statistical analysis

All statistical analyses were performed using Python 3.13 with the following packages: pyDESeq2 for differential expression, scikit-learn for LASSO and machine learning, lifelines for survival analysis, gseapy for GSEA, and scipy/statsmodels for statistical tests. The Wilcoxon rank-sum test was used for two-

group comparisons; the Kruskal–Wallis test for multiple groups. Spearman correlation was used for non-parametric correlation analysis. The chi-squared test was used for categorical variables. $P < 0.05$ was considered statistically significant. Analyses were restricted to samples with complete data for the variables involved in each analysis (complete-case approach); no imputation was performed.

Results

Identification of differentially expressed anesthesia-related genes in colorectal cancer

To identify ARGs differentially expressed between tumor and normal colorectal tissues, we first compiled an ARG catalog from two sources: (i) genes differentially expressed in glioblastoma tissue resected under propofol versus sevoflurane anesthesia (GSE179004, $|\log_2 FC| > 0.5$, $P < 0.05$), and (ii) genes with established links to anesthetic agents from a systematic literature review. After intersecting with the TCGA-CRC gene list, we obtained approximately 200 unique ARGs represented on the platform.

Differential expression analysis was performed on the TCGA-CRC cohort (649 tumors, 51 adjacent normal tissues) using DESeq2. Among 54,437 genes tested, 14,190 were differentially expressed ($|\log_2 FC| > 1$, adjusted $P < 0.05$). Intersecting these DEGs with the ARG catalog yielded 78 differentially expressed anesthesia-related genes (DEARGs), comprising 42 upregulated and 36 downregulated genes in tumors relative to normal tissues (Fig. 1A; Supplementary Table S1). Among the most prominently upregulated DEARGs were *GABRP* ($\log_2 FC = 3.02$, $P_{adj} = 9.0 \times 10^{-20}$), *GABRA3* ($\log_2 FC = 2.20$, $P_{adj} = 2.5 \times 10^{-5}$), and *DRD4* ($\log_2 FC = 1.01$, $P_{adj} = 1.3 \times 10^{-7}$), while *CHRNA3* ($\log_2 FC = -2.06$, $P_{adj} = 2.2 \times 10^{-17}$) and *EPHX2* ($\log_2 FC = -1.38$, $P_{adj} = 3.3 \times 10^{-12}$) were among the most strongly downregulated.

KEGG pathway enrichment analysis of the 78 DEARGs revealed significant enrichment in pathways directly relevant to anesthetic mechanisms, including nicotine addiction (adjusted $P = 1.0 \times 10^{-24}$, 15/40 genes), GABAergic synapse (adjusted $P = 2.3 \times 10^{-12}$, 11/89 genes), morphine addiction (adjusted $P = 1.8 \times 10^{-9}$, 9/91 genes), and dopaminergic synapse (adjusted $P = 3.5 \times 10^{-8}$, 9/132 genes) (Fig. 2D; Supplementary Table S2). Additional enriched pathways included calcium signaling, retrograde endocannabinoid signaling, and the p53 signaling pathway, all of which are biologically connected to anesthetic drug targets and tumor progression.

Construction of a 15-gene anesthesia-related prognostic signature

For model development, the 78 DEARGs were filtered to 35 genes with measurable expression across the analyzed platforms. Univariate Cox screening followed by L1-penalized Cox regression with 10-fold cross-validation was used to derive a 15-gene model. Because feature screening and performance

assessment were conducted within the same development cohort, internal estimates may be optimistic; the external cohorts provide the principal assessment of transportability.

Univariate Cox regression on the TCGA training cohort identified 3 genes with $P < 0.05$: GABRD (HR = 1.38, $P = 9.3 \times 10^{-5}$), DRD4 (HR = 1.32, $P = 1.3 \times 10^{-3}$), and CDKN2A (HR = 1.22, P = 0.014). L1-penalized Cox regression (lifelines CoxPHFitter with L1 penalty, 10-fold cross-validation) was then applied to the 35 candidate genes to select the optimal feature set and shrink coefficients. The final model retained 15 genes with non-zero coefficients (Fig. 1B):

Risk score = (− 0.245 × CACNA1D) + (− 0.214 × CCNE1) + (0.182 × DRD4) + (0.173 × GABRD) + (0.146 × VEGFA) + (− 0.120 × EPHX2) + (− 0.114 × CHRNA1) + (0.108 × GABRE) + (0.097 × KCNMA1) + (0.085 × CDKN2A) + (0.061 × AQP1) + (− 0.052 × PHKG1) + (0.046 × GLRB) + (0.014 × CACNA1C) + (0.010 × ITPKB)

Five genes (CACNA1D, CCNE1, EPHX2, CHRNA1, PHKG1) carried negative coefficients, indicating a protective association, while ten genes (DRD4, GABRD, VEGFA, GABRE, KCNMA1, CDKN2A, AQP1, GLRB, CACNA1C, ITPKB) were risk factors. The model incorporated genes spanning voltage-gated calcium channels (CACNA1D, CACNA1C), GABAA receptor subunits (GABRD, GABRE), nicotinic acetylcholine receptors (CHRNA1), dopamine receptors (DRD4), potassium channels (KCNMA1), and cell cycle regulators (CDKN2A, CCNE1), reflecting the biological diversity of anesthetic targets implicated in CRC progression. TCGA-CRC patients were stratified into high-risk (n = 295) and low-risk (n = 295) groups using the median risk score as the cutoff. A coefficient-preserving sensitivity analysis decomposed the 15-gene model by ARG source: the 11 literature-curated genes yielded a C-index of 0.663 on TCGA, the 4 GSE179004-only genes yielded a C-index of 0.611, and the Spearman correlation between the two sub-scores was $\rho = 0.306$ ($P = 3.1 \times 10^{-14}$), indicating that both source subsets contributed complementary prognostic signal and that the full 15-gene C-index of 0.682 reflects an additive effect rather than dependence on a single source.

Apparent prognostic performance in TCGA and external cohorts

In the TCGA-CRC training cohort, Kaplan–Meier analysis demonstrated that patients in the high-risk group had significantly worse overall survival than those in the low-risk group (log-rank $P = 1.5 \times 10^{-8}$; Fig. 1D). The concordance index (C-index) was 0.682, indicating moderate apparent discrimination.

Univariate Cox regression confirmed that the risk score was a significant predictor of survival (HR = 2.91, 95% CI: 1.98–4.27, $P = 4.7 \times 10^{-8}$). To assess whether the risk score was independent of established clinical covariates, we performed multivariate Cox regression adjusting for age, sex, TNM stage, T classification, N classification, and M classification. The risk score remained an independent prognostic factor (HR = 2.27, 95% CI: 1.51–3.43, $P = 9.3 \times 10^{-5}$), whereas T, N, and M classifications lost significance in the multivariate model, with only TNM stage retaining marginal significance (HR = 2.80, P = 0.025) (Fig. 2A, Table 1).

Time-dependent ROC analysis yielded AUC values of 0.715 at 1 year, 0.707 at 3 years, and 0.758 at 5 years (Fig. 2B), demonstrating that the model maintained predictive accuracy across clinically relevant follow-up intervals.

The model was evaluated in two GEO cohorts with different survival endpoints. In GSE17536 (n = 145), C-indices ranged from 0.618 to 0.681 across disease-free and disease-specific survival analyses. In GSE39582 (n = 557), the relapse-free-survival C-index was 0.535 under rank-based normalization, close to chance discrimination. Platform, endpoint, treatment, follow-up, preprocessing, and overfitting differences may all contribute; the available analyses do not isolate a single cause. This result indicates weak transportability and requires independent recalibration and validation.

Table 1
Univariate and multivariate Cox regression analysis of prognostic factors in TCGA-CRC.

Variable	HR	95% CI	P value	Analysis
Risk score	2.909	1.983–4.268	4.74e-08	Univariate
TNM Stage	2.469	1.892–3.222	2.82e-11	Univariate
T classification	3.023	1.312–6.965	0.009	Univariate
N classification	2.648	1.672–4.192	3.28e-05	Univariate
M classification	5.641	3.540–8.988	3.35e-13	Univariate
Risk score	2.271	1.505–3.427	9.26e-05	Multivariate
TNM Stage	2.797	1.141–6.857	0.025	Multivariate
T classification	0.799	0.291–2.195	0.663	Multivariate
N classification	0.503	0.197–1.285	0.151	Multivariate
M classification	1.166	0.354–3.836	0.801	Multivariate

Association between the risk score and clinicopathological features

The risk score was significantly associated with advanced disease stage (stage I/II vs. III/IV, Mann–Whitney $P = 1.1 \times 10^{-8}$), T classification (T1–T2 vs. T3–T4, $P = 1.0 \times 10^{-4}$), N classification (N0 vs. N1–N2, $P = 1.5 \times 10^{-9}$), and M classification (M0 vs. M1, $P = 1.9 \times 10^{-4}$) (Fig. 2C). Patients with more advanced tumors exhibited higher risk scores, consistent with the model capturing biologically aggressive disease features.

Tumor immune microenvironment characteristics in high- versus low-risk tumors

Given the emerging evidence associating anesthetic agents with antitumor immune characteristics, we next compared the immune cell composition between risk groups using CIBERSORT deconvolution of the TCGA-CRC transcriptome. Five immune cell types were significantly different between groups (Fig. 3A). High-risk tumors harbored higher proportions of M0 macrophages (mean difference = 1,118; $P = 8.6 \times 10^{-8}$), monocytes ($P = 4.5 \times 10^{-5}$), M2 macrophages ($P = 2.0 \times 10^{-4}$), activated mast cells ($P = 0.035$), and regulatory T cells (Tregs; $P = 0.038$). The enrichment of immunosuppressive cell populations—particularly M2 macrophages and Tregs—in high-risk tumors was consistent with an immune-excluded or suppressive phenotype.

ESTIMATE (Estimation of STromal and Immune cells in MAlignant Tumor tissues using Expression data) analysis corroborated these findings. Stromal scores were substantially elevated in high-risk tumors ($P = 4.0 \times 10^{-12}$), as were ESTIMATE scores ($P = 3.9 \times 10^{-8}$), while immune scores showed a more modest increase ($P = 0.014$) (Fig. 3B). The disproportionately higher stromal component indicated that the high-risk microenvironment is characterized by altered stromal composition rather than a simple increase in immune infiltration.

In silico immune-response proxy analyses

TIDE-derived dysfunction and exclusion scores differed between risk groups, with higher mean exclusion and overall TIDE scores in the high-risk group (Fig. 3C). A threshold-derived proxy classification also differed between groups. Because these are algorithmic scores rather than observed outcomes, they do not establish differential response to immune checkpoint blockade and require evaluation in clinically annotated CRC immunotherapy cohorts.

The Immunophenoscore (IPS) was also computed. The overall IPS did not differ between groups, whereas the suppressor-cell component was higher in the high-risk group (Fig. 3D). IPS-derived CTLA-4 and PD-1 proxy classifications varied across risk groups, but these exploratory categories should not be interpreted as responder rates or treatment recommendations.

Tumor mutation burden (TMB; non-synonymous mutations per megabase) was weakly but significantly inversely correlated with the risk score (Spearman $\rho = -0.106$, $P = 0.011$), though the median TMB did not differ significantly between groups (2.29 vs. 2.42 mut/Mb, $P = 0.156$).

GSEA reveals metabolic and proliferative reprogramming in high-risk tumors

Gene set enrichment analysis (GSEA) was performed on 20,822 genes ranked by the signal-to-noise ratio between high- and low-risk groups across three gene set collections (MSigDB Hallmark, KEGG, Reactome) with 1,000 permutations. A total of 434 pathways reached nominal significance (FDR < 0.25), of which 16 were strictly significant (FDR < 0.05) (Fig. 4A; Supplementary Table S4).

High-risk tumors exhibited coordinated upregulation of biosynthetic and bioenergetic pathways, including Myc target genes (NES = 2.02, FDR = 0.021), E2F target genes (NES = 1.93, FDR = 0.033),

oxidative phosphorylation (NES = 2.06, FDR = 0.029), the tricarboxylic acid (TCA) cycle (NES = 2.00, FDR = 0.032), pyruvate metabolism (NES = 2.02, FDR = 0.031), and fatty acid degradation (NES = 1.94, FDR = 0.034). Mitochondrial protein degradation (NES = 2.33, FDR = 0.017) was the most strongly enriched Reactome pathway in high-risk tumors. These results indicate that high-risk CRC is metabolically hyperactive, with accelerated mitochondrial respiration, biomass precursor synthesis, and cell cycle progression.

In contrast, low-risk tumors were enriched in pathways associated with stromal and vascular programs, including angiogenesis (NES = − 1.86, FDR = 0.063), myogenesis (NES = − 2.01, FDR = 0.068), epithelial–mesenchymal transition (EMT; NES = − 1.89, FDR = 0.103), and apical junction (NES = − 1.87, FDR = 0.081). Although these pathways did not reach the FDR < 0.05 threshold, the consistent directionality suggests that low-risk tumors may retain features of differentiated epithelial architecture and vascular normalization.

Drug sensitivity profiling and potential therapeutic agents

Using the oncoPredict algorithm trained on GDSC2 pharmacogenomic data (805 cell lines, 183 drugs), we compared predicted IC_{50} values between high- and low-risk groups. Of 183 drugs tested, 117 showed significant differences ($P < 0.05$) and 115 remained significant after Benjamini–Hochberg correction (Fig. 4B; Supplementary Table S5).

Among selected anticancer agents, predicted IC50 values differed between risk groups for cisplatin, topotecan, sorafenib, erlotinib, docetaxel, and selumetinib (Fig. 4C). These in silico estimates were derived from cell-line-trained models and were not evaluated against patient treatment response; they generate pharmacologic hypotheses but do not support drug selection.

Model gene expression correlates with inferred immune-cell scores

To explore associations between model genes and inferred immune populations, we correlated bulk-tumor gene expression with ssGSEA-derived immune-cell scores. These analyses do not localize gene expression to individual cell types and should not be interpreted as single-cell evidence.

Several model genes correlated with ssGSEA-derived immune-cell scores, including positive associations of KCNMA1, GLRB, AQP1, and ITPKB with macrophage- and mast-cell signatures and inverse associations of CACNA1D and VEGFA with several immune scores. These are bulk-expression correlations that may reflect tumor purity, stromal composition, or shared transcriptional programs; they do not demonstrate expression by a specific immune-cell population or causal immune regulation.

Protein-level corroboration using the Human Protein Atlas

To corroborate our transcriptome-based findings at the protein level, we queried the Human Protein Atlas (HPA) for immunohistochemistry (IHC) data on the 15 model genes in CRC tissue (Fig. 5C;

Supplementary Table S7). Ten of 15 genes (66.7%) had detectable protein expression in CRC samples: VEGFA (moderate-to-strong cytoplasmic staining), AQP1 (moderate-to-strong cytoplasmic/membrane staining), EPHX2 (moderate cytoplasmic), CCNE1 (weak-to-moderate nuclear), CDKN2A (weak-to-moderate nuclear and cytoplasmic), KCNMA1 (weak-to-moderate cytoplasmic/membrane), CACNA1D (weak cytoplasmic), GABRD (weak cytoplasmic), PHKG1 (weak cytoplasmic), and ITPKB (moderate cytoplasmic).

CDKN2A (p16INK4a) was annotated in HPA as an unfavorable prognostic marker in colon adenocarcinoma. This separate database annotation is supportive context, not an independent validation of the multigene risk model.

Summary of the 15-gene model

The final 15-gene signature integrates genes from multiple anesthetic-relevant functional categories (Fig. 5C, Table 2): ligand-gated ion channels (GABRD, GABRE, CHRNA1, GLRB), voltage-gated calcium channels (CACNA1D, CACNA1C), a voltage-gated potassium channel (KCNMA1), G protein-coupled receptors (DRD4), cell cycle regulators (CDKN2A, CCNE1), a pro-angiogenic factor (VEGFA), an aquaporin channel (AQP1), an epoxyhydrolase (EPHX2), a phosphorylase kinase subunit (PHKG1), and an inositol kinase (ITPKB). The diversity of functional classes represented in the model—spanning the very targets through which anesthetics exert their pharmacological effects—supports the premise that anesthesia-associated molecular pathways are relevant to CRC biology as a hypothesis-generating framework.

Table 2
Summary of the 15-gene anesthesia-related prognostic signature.

Gene	Coefficient	HR	Direction	Functional Category	HPA IHC (CRC)	HPA Prognostic Marker
CACNA1D	-0.2449	0.7828	Protective	Voltage-gated Ca^{2+} channel	Weak	Not reported
CCNE1	-0.2136	0.8076	Protective	Cell cycle regulator	Weak-Moderate	Yes (multiple studies)
DRD4	0.1823	1.2000	Risk	Dopamine receptor (GPCR)	Not detected	Not reported
GABRD	0.1733	1.1892	Risk	GABA receptor subunit	Weak	Not reported
VEGFA	0.1458	1.1569	Risk	Pro-angiogenic factor	Moderate-Strong	No
EPHX2	-0.1198	0.8871	Protective	Epoxyhydrolase	Moderate	Not reported
CHRNA1	-0.1144	0.8919	Protective	Nicotinic ACh receptor	Not detected	Not reported
GABRE	0.1080	1.1141	Risk	GABA receptor subunit	Not detected	Not reported
KCNMA1	0.0966	1.1014	Risk	Voltage-gated K^+ channel	Weak-Moderate	Not reported
CDKN2A	0.0848	1.0885	Risk	Cell cycle regulator (p16)	Weak-Moderate	Yes (COAD, $P < 0.001$)
AQP1	0.0605	1.0624	Risk	Aquaporin channel	Moderate-Strong	Not reported
PHKG1	-0.0525	0.9489	Protective	Phosphorylase kinase subunit	Weak	Not reported
GLRB	0.0463	1.0474	Risk	Glycine receptor subunit	Not detected	Not reported
CACNA1C	0.0138	1.0139	Risk	Voltage-gated Ca^{2+} channel	Not detected	Not reported
ITPKB	0.0099	1.0099	Risk	Inositol kinase	Moderate	Not reported

Discussion

In this study, we developed and externally evaluated a 15-gene signature derived from anesthesia-related candidate genes in colorectal cancer. The signature showed moderate apparent discrimination in TCGA and GSE17536 but weak performance in GSE39582, which materially limits claims of generalizability.

The ARG catalog combined an exploratory six-sample glioblastoma expression comparison with literature-curated genes. The small, non-CRC discovery set and nominal-P screening create substantial tissue-specific and false-positive risk. The catalog should therefore be considered a hypothesis-generating starting set rather than evidence that the included genes mediate anesthetic effects in CRC. The 11 literature-curated and 4 GSE179004-derived genes in the model are not equally distributed across functional categories (literature genes dominate neurotransmitter receptor and ion channel families; GSE genes include AQP1, CACNA1C, ITPKB, and DRD4), and the source-decomposition analysis (C-index 0.663 vs. 0.611) suggests that both arms contributed to the full-model performance, although neither subset alone reached the full-model C-index.

The 15-gene model incorporates genes from diverse functional categories representing the pharmacological targets of anesthetics. GABA-A receptor subunits (GABRD, GABRE) and nicotinic acetylcholine receptors (CHRNA1) are pharmacological targets of propofol and sevoflurane [10–12]. Voltage-gated calcium channels (CACNA1D, CACNA1C) and the potassium channel KCNMA1 are associated with cancer cell proliferation and migration [13–15]. CDKN2A (p16INK4a), a well-established tumor suppressor and CRC prognostic biomarker annotated by the Human Protein Atlas, and CCNE1 (cyclin E1) link the signature to cell cycle regulation. VEGFA, AQP1, and EPHX2 are associated with angiogenesis, fluid balance, and oxidative metabolism, respectively. The inclusion of these functionally diverse genes supports the premise that anesthesia-associated molecular pathways are relevant to CRC biology.

It is important to acknowledge that the risk score was significantly associated with advanced TNM stage, T classification, and N classification (all $P < 0.001$), and that T, N, and M classifications lost significance in multivariate Cox regression when the risk score was included. This suggests that the signature may function as a transcriptomic proxy for tumor burden and aggressiveness, rather than a purely independent biological axis. The model likely captures downstream transcriptional programs associated with tumor aggressiveness and disease progression. The model likely reflects downstream transcriptional consequences of tumor advancement—including activation of proliferation, metabolic reprogramming, and immune remodeling—rather than direct causal effects of anesthetic exposure on CRC. Accordingly, we have refrained from claiming that anesthetic agents directly regulate CRC progression. Instead, the risk score should be interpreted as a composite transcriptomic marker that integrates prognostic information from neuroactive ligand-receptor pathways with broader tumor biology, offering additive prognostic value beyond TNM stage, as supported by the multivariate model (HR = 2.27, P = 9.3 x 10^-5) and the time-dependent AUC (5-year AUC = 0.758).

The immune microenvironment analysis associated the high-risk group with higher inferred M2 macrophage, monocyte, regulatory T-cell, and stromal scores. TIDE and IPS also differed between risk groups, but these are computational proxy scores rather than observed treatment responses. No CRC-specific bulk RNA-seq immunotherapy cohort with matched clinical response was analyzed, so the findings should be framed as hypotheses for future validation rather than evidence of immunotherapy benefit.

Drug-sensitivity modeling identified compounds with differential predicted IC50 values between risk groups. These computational estimates are exploratory and require concentration-response testing and clinically annotated validation; they do not support treatment selection.

From a perioperative perspective, the 15-gene score offers a candidate stratification biomarker for future prospective trials that compare anesthetic regimens in CRC surgery, although the present data do not support any specific agent choice. The published literature on propofol- versus volatile-anesthesia long-term oncologic outcomes remains mixed: intravenous propofol-based anesthesia has been associated with attenuated perioperative immunosuppression and reduced circulating VEGF in some surgical cohorts [3, 6], while large retrospective series in colorectal and other gastrointestinal cancers have generally not shown a consistent survival difference between propofol and sevoflurane regimens [1, 2, 4]. A molecular biomarker such as the 15-gene score would in principle allow future randomized studies to pre-specify a high-risk subgroup in which any agent effect on recurrence or immune recovery could be detectable, while a low-risk subgroup could serve as a negative control, mirroring the biomarker-enriched design increasingly recommended for perioperative oncology trials. Whether the ARG-based risk score is reproducible on clinically available assays (for example, RNA extracted from formalin-fixed paraffin-embedded resection specimens or pre-operative biopsies) and whether it responds to anesthetic exposure in vivo are open questions that require prespecified analytical validation before any such trial can be designed.

A critical observation is that the 15-gene signature showed weak discrimination in GSE39582 (C-index 0.535), close to chance. The available analyses cannot distinguish among platform shift, cohort and endpoint heterogeneity, preprocessing differences, and model overfitting. This result indicates limited transportability and should be treated as a central limitation rather than attributed to microarray technology alone. Recalibration and evaluation in independent RNA-seq and prospectively specified assay cohorts are needed.

Limitations

Several limitations should be acknowledged. First, the ARG catalog included an exploratory glioblastoma microarray comparison with only six samples and nominal-P screening, creating tissue-specific and false-positive risk. Second, feature screening, model fitting, and internal performance assessment were not fully separated, so development estimates may be optimistic. Third, external performance was inconsistent and approached chance in GSE39582. Fourth, immune-cell estimates, TIDE, IPS, and drug-sensitivity results are computational proxies without clinical response validation. Fifth, HPA staining is database corroboration rather than experimental validation of the risk model. Sixth, detailed treatment information and functional experiments were unavailable. These constraints preclude causal or clinical claims and motivate prespecified validation with locked coefficients, complete sample manifests, calibration assessment, and laboratory testing.

Conclusions

This retrospective bioinformatics study identified a 15-gene ARG signature associated with outcome and inferred immune phenotypes in colorectal cancer. The TCGA association remained after clinical adjustment, but external performance was inconsistent and approached chance in GSE39582. TIDE/IPS, oncoPredict, and HPA analyses should be regarded as hypothesis-generating. The model is not ready for clinical use; independent RNA-seq cohorts, prespecified calibration, and functional validation are required.

Abbreviations

ARGs
Anesthesia-related genes
AUC
Area under the curve
CIBERSORT
Cell type Identification By Estimating Relative Subsets Of RNA Transcripts
CRC
Colorectal cancer
DEARGs
Differentially expressed anesthesia-related genes
DFS
Disease-free survival
DSS
Disease-specific survival
ESTIMATE
Estimation of STromal and Immune cells in MAlignant Tumor tissues using Expression data
FDR
False discovery rate
GSEA
Gene set enrichment analysis
HPA
Human Protein Atlas
IC50
Half-maximal inhibitory concentration
ICI
Immune checkpoint inhibitor
IPS
Immunophenoscore
MAF
Mutation annotation format
MSI

Microsatellite instability
MSI-H
Microsatellite instability-high
MSS
Microsatellite stable
NES
Normalized enrichment score
ORR
Objective response rate
OS
Overall survival
PFS
Progression-free survival
qPCR
Quantitative polymerase chain reaction
RFS
Relapse-free survival
ROC
Receiver operating characteristic
ssGSEA
Single-sample gene set enrichment analysis
TIDE
Tumor Immune Dysfunction and Exclusion
TMB
Tumor mutation burden
TCGA
The Cancer Genome Atlas
GEO
Gene Expression Omnibus
GDSC
Genomics of Drug Sensitivity in Cancer.

Declarations

Ethics approval and consent to participate

Not applicable. This study analyzed de-identified data from publicly accessible repositories and did not involve prospective recruitment, intervention, or new collection of human specimens.

Consent for publication

Not applicable.

Competing interests

The authors declare that they have no competing interests.

Funding

This work received no specific grant from any funding agency in the public, commercial, or not-for-profit sectors.

Author Contribution

Yu Zhang designed the study, performed the bioinformatics analyses, and drafted the manuscript. Wangyang Zhang participated in data collection and interpretation and critically revised the manuscript. Meng Sha assisted with data analysis and interpretation. Weixian Xie and Qiang Wang supervised the project, provided methodological guidance, and approved the final version. All authors read and approved the final manuscript.

Acknowledgements

The authors thank the TCGA, GEO, GDSC, and HPA databases for providing open access to their data resources.

Data Availability

All data analyzed in this study are publicly available. Direct access links and accession identifiers for each dataset are listed below:TCGA-COAD (colon adenocarcinoma; RNA-seq counts, clinical and mutation data): https://portal.gdc.cancer.gov/projects/TCGA-COADTCGA-READ (rectum adenocarcinoma; RNA-seq counts, clinical and mutation data): https://portal.gdc.cancer.gov/projects/TCGA-READGDC Data Portal API (batch download of primary data): https://api.gdc.cancer.gov/dataUCSC Xena (TCGA-COAD/READ phenotype and survival data): https://xenabrowser.net/datapages/?cohort=TCGA%20Colon%20Cancer%20(COAD); https://xenabrowser.net/datapages/?cohort=TCGA%20Rectal%20Cancer%20(READ)GEO GSE39582 (validation cohort, CRC): https://www.ncbi.nlm.nih.gov/geo/query/acc.cgi?acc=GSE39582GEO GSE17536 (validation cohort, CRC): https://www.ncbi.nlm.nih.gov/geo/query/acc.cgi?

acc=GSE17536GEO GSE179004 (propofol- vs sevoflurane-exposed samples; source of anesthesia-related genes): https://www.ncbi.nlm.nih.gov/geo/query/acc.cgi?acc=GSE179004GDSC2 (drug-response training data for oncoPredict, OSF repository "DataFiles"): https://osf.io/c6tfx/CIBERSORT (LM22 signature matrix, CIBERSORTx portal): https://cibersortx.stanford.edu/ESTIMATE (StromalScore/ImmuneScore): https://sourceforge.net/projects/estimateproject/TIDE (Tumor Immune Dysfunction and Exclusion algorithm; Jiang et al., Nat Med 2018; original portal http://tide.dfci.harvard.edu/ has since been retired and its modules are now maintained as the Cancer Immunology Data Engine, https://cide.ccr.cancer.gov/, with the response-prediction module available as the TIDEpy Python package)Enrichr (GO/KEGG enrichment analysis): https://maayanlab.cloud/Enrichr/MSigDB (Hallmark gene sets for GSEA): https://www.gsea-msigdb.org/gsea/msigdb/collections.jspHuman Protein Atlas (protein expression annotation): https://www.proteinatlas.org/Analysis scripts, model coefficients, sample manifests, and intermediate result tables (LASSO coefficients, immune-cell fractions, drug-sensitivity predictions) are available from the corresponding author on reasonable request and will be deposited in a public repository (e.g., Zenodo or GitHub) with a DOI assigned at the time of article acceptance.

References

1. Wigmore TJ, Mohammed K, Jhanji S. Long-term survival for patients undergoing volatile versus IV anesthesia for cancer surgery: a retrospective analysis. Anesthesiology. 2016;124(1):69–79.
2. Sessler DI, Riedel B. Anesthesia and cancer recurrence: context for divergent study outcomes. Anesthesiology. 2019;130(1):3–5. 10.1097/ALN.0000000000002506.
3. Sekandarzad MW, van Zundert AAJ, Lirk PB, Doornebal CW, Hollmann MW. Perioperative anesthesia care and tumor progression. Int Anesthesiol Clin. 2016;54(4):e1–16.
4. Tavare AN, O'Dell G, O'Leary E, et al. Perioperative anesthetic regimen and long-term outcome after cancer surgery. J Clin Anesth. 2018;49:53–60.
5. Huang H, Benzonana LL, Zhao H, et al. Prostate cancer cell malignancy via modulation of HIF-1α pathway with isoflurane and propofol alone and in combination. Br J Cancer. 2014;111(7):1338–49. 10.1038/bjc.2014.451.
6. Jiang S, Liu Y, Huang L, Zhang F, Kang R. Effects of propofol on cancer development and chemotherapy: potential mechanisms. Eur J Pharmacol. 2018;831:46–51. 10.1016/j.ejphar.2018.04.009.
7. Battaglin F, Jayachandran P, Strelez C, et al. Neurotransmitter signaling: a new frontier in colorectal cancer biology and treatment. Oncogene. 2022;41(43):4769–78. 10.1038/s41388-022-02479-4.
8. Grant CE, Flis AL, Ryan BM. Understanding the role of dopamine in cancer: past, present and future. Carcinogenesis. 2022;43(6):517–27. 10.1093/carcin/bgac045.
9. Keane JM, Fernandes P, Kratz F, et al. Interplay between microbial-derived GABA and host GABA receptor signaling collectively influence the tumorigenic function of GABA in colon cancer. Pharmacol Res Perspect. 2024;12(3):e1226. 10.1002/prp2.1226.

10. Yamakura T, Bertaccini E, Trudell JR, Harris RA. Anesthetics and ion channels: molecular models and sites of action. Annu Rev Pharmacol Toxicol. 2001;41:23–51. 10.1146/annurev.pharmtox.41.1.23.
11. Meng C, Song L, Wang J, Li D, Liu Y, Cui X. Propofol induces proliferation partially via downregulation of p53 protein and promotes migration via activation of the Nrf2 pathway in the human breast cancer cell line MDA-MB-231. Oncol Rep. 2017;37(2):841–8. 10.3892/or.2016.5332.
12. Grando SA. Connections of nicotine to cancer. Nat Rev Cancer. 2014;14(6):419–29. 10.1038/nrc3725.
13. Buchanan PJ, McCloskey KD. CaV channels and cancer: canonical functions indicate benefits of repurposed drugs as cancer therapeutics. Eur Biophys J. 2016;45(7):621–33. 10.1007/s00249-016-1144-z.
14. Ibrahim S, Dakik H, Vandier C, et al. Expression profiling of calcium channels and calcium-activated potassium channels in colorectal cancer. Cancers (Basel). 2019;11(4):561. 10.3390/cancers11040561.
15. Ohya S, Kajikuri J, Kito H, Matsui M. Down-regulation of CYP3A4 by the KCa1.1 inhibition is responsible for overcoming resistance to doxorubicin in cancer spheroid models. Int J Mol Sci. 2023;24(21):15672. 10.3390/ijms242115672.

Figures

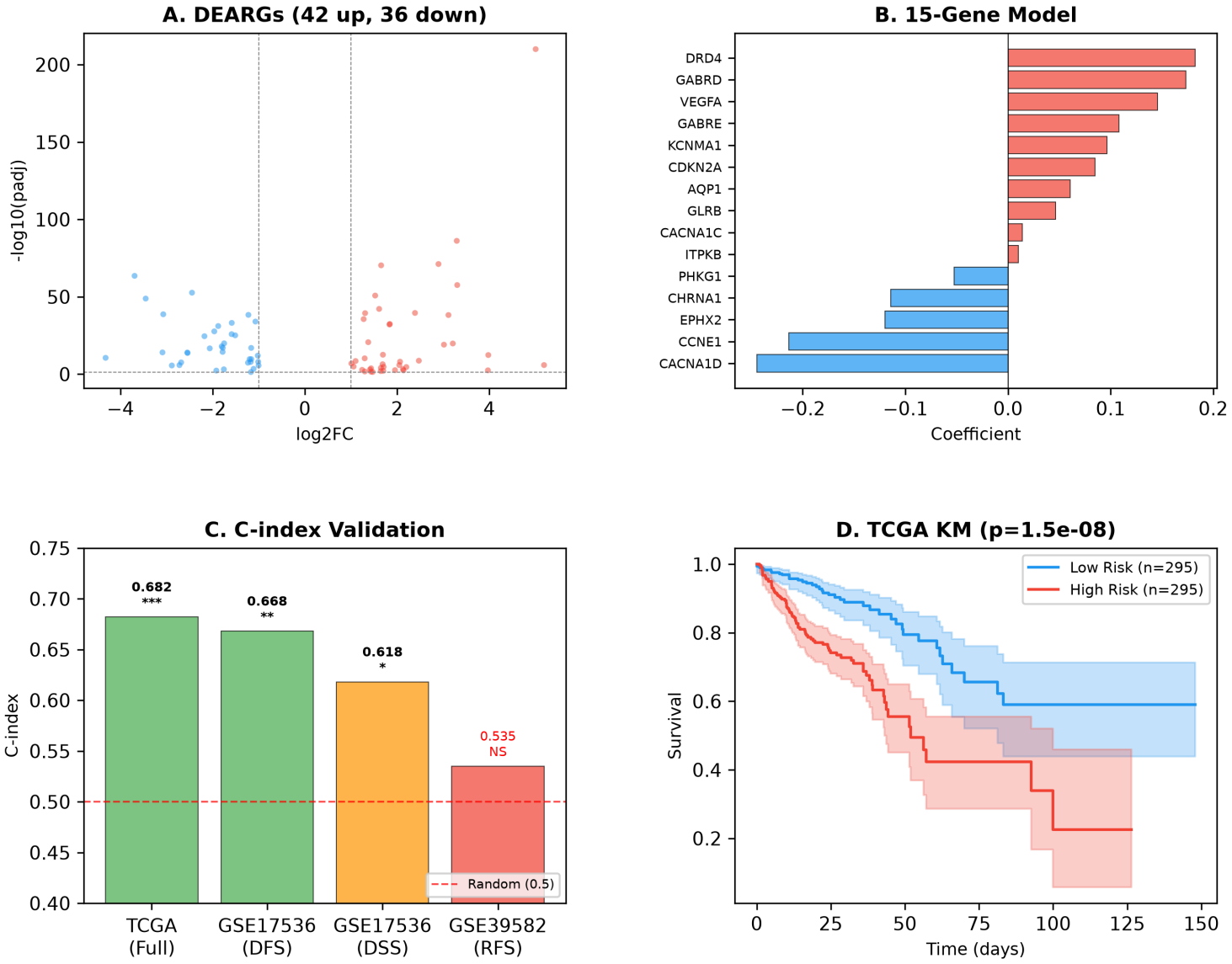


Figure 1

DEARGs and 15-gene model construction. (A) Volcano plot of 78 differentially expressed anesthesia-related genes (DEARGs) in TCGA-CRC ($|\log_2 FC| > 1$, adjusted $P < 0.05$). Red: upregulated; blue: downregulated. (B) LASSO regression coefficients for the 15 model genes, sorted by magnitude. (C) Concordance-index (C-index) evaluation across TCGA (OS), GSE17536 (DFS, DSS) and GSE39582 (RFS); dashed red line denotes random (0.5). (D) Kaplan–Meier overall-survival curves for TCGA-CRC patients stratified by median risk score (log-rank $P = 1.5 \times 10^{-8}$).

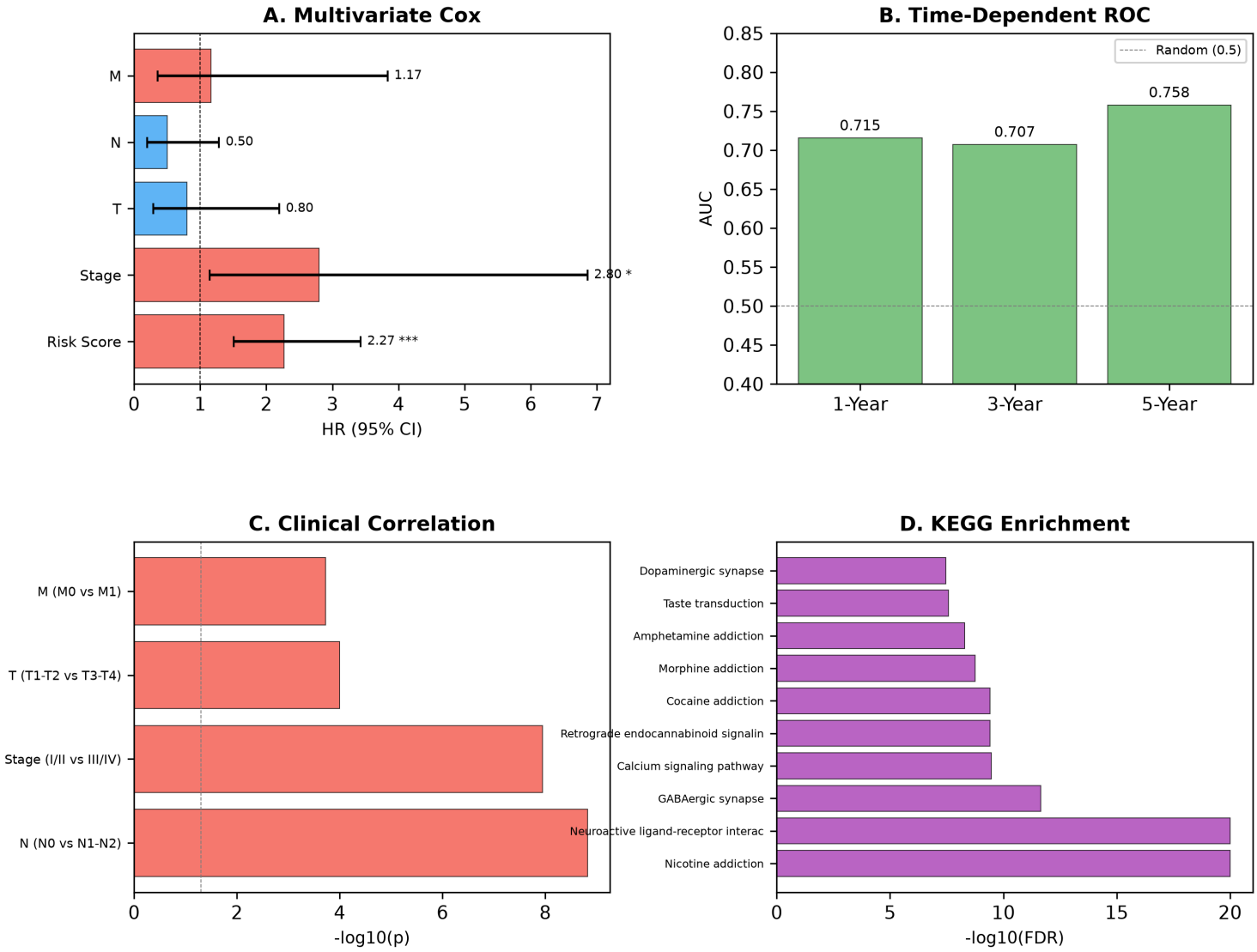


Figure 2

Prognostic evaluation, clinical correlation and pathway enrichment of the 15-gene signature. (A) Multivariate Cox forest plot showing risk score as an independent prognostic factor (HR = 2.27, P = 9.3 × 10^{-5}) after adjustment for age, sex, TNM stage, T, N and M classifications. (B) Time-dependent ROC curves at 1, 3, and 5 years (AUC = 0.715, 0.707, 0.758). (C) Clinical feature correlation with risk score (–log10 P). (D) KEGG pathway enrichment of 78 DEARGs (top 10 by –log10 FDR).

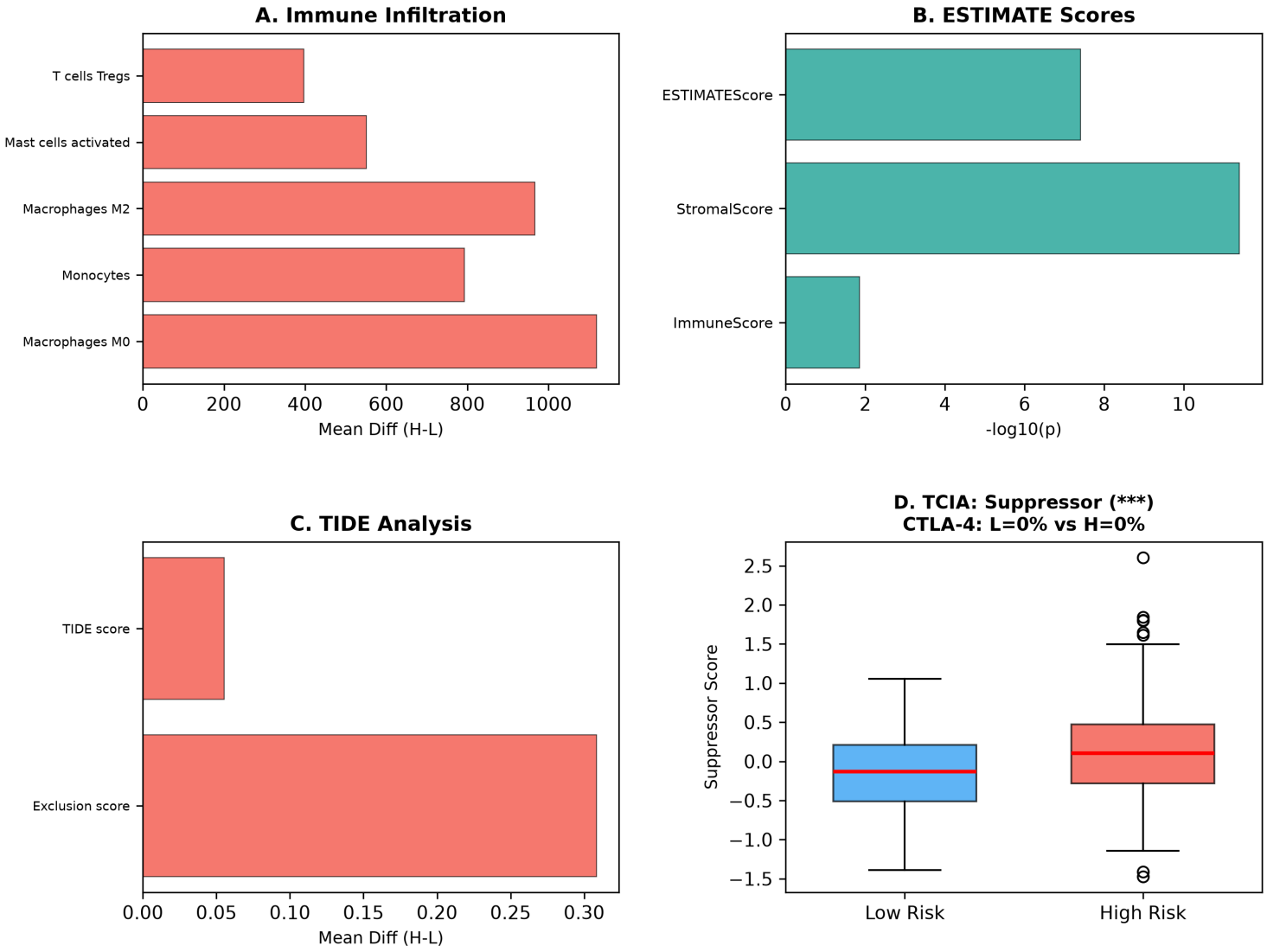


Figure 3

Inferred tumor immune microenvironment characteristics and immune-response proxy scores. (A) CIBERSORT immune-cell infiltration differences between high- and low-risk groups (mean difference H–L). (B) ESTIMATE algorithm comparison: ImmuneScore, StromalScore, and ESTIMATEScore (–log10 P). (C) TIDE immune-exclusion and overall TIDE score differences (H–L). (D) TCIA Immunophenoscore (IPS) Suppressor component in low versus high risk (***, $P = 3.6 \times 10^{-7}$).

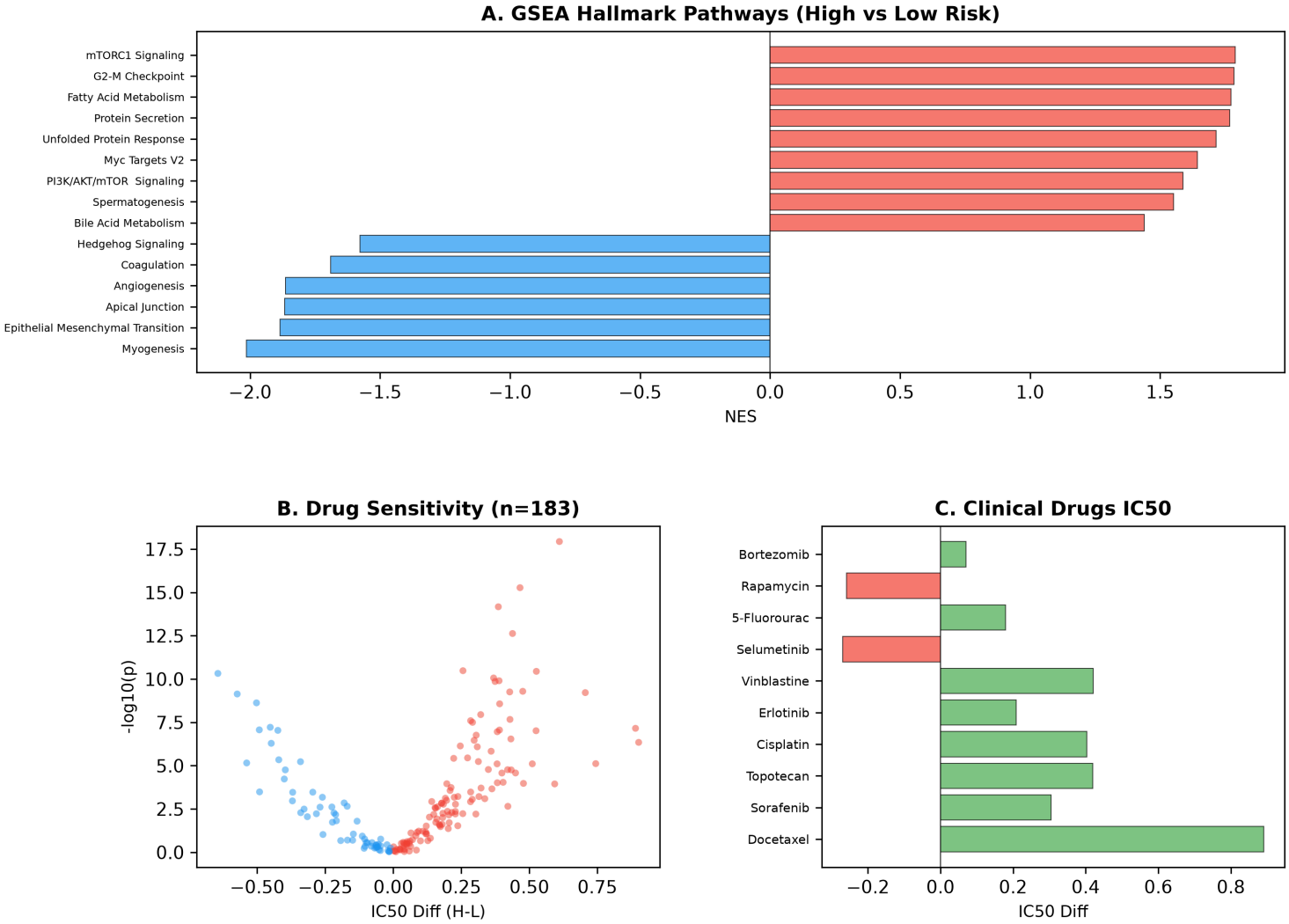
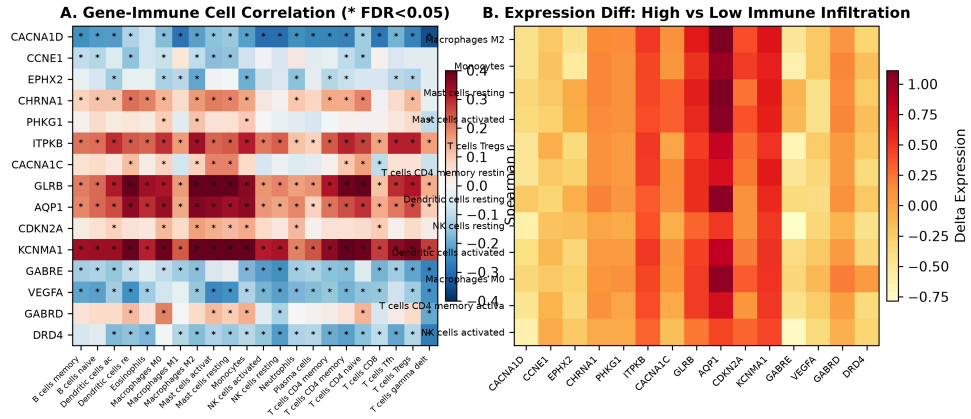


Figure 4

Pathway enrichment and drug-sensitivity analysis. (A) GSEA Hallmark pathway enrichment for high versus low risk (top 15 by NES). (B) Volcano plot of predicted IC_{50} differences between risk groups for 183 GDSC2 drugs (−log10 P vs. IC_{50} difference H−L). (C) IC_{50} differences for clinically relevant CRC therapeutics.



C. 15-Gene Model Summary: Coefficients, HPA IHC Evidence, and Anesthesia-Related Function

Gene	Coefficient	Direction	HPA IHC (CRC)	HPA Prognostic Marker	ARG Type	Function
CACNA1D	-0.2449	Protective	Weak		Ca2+ channel	L-type Ca2+ ch.
CCNE1	-0.2136	Protective	Weak-Mod		Cell cycle	Cyclin E1
DRD4	0.1823	Risk	Not det.		Dopamine receptor	D4 dopamine
GABRD	0.1733	Risk	Weak		GABA receptor	delta GABA-A
VEGFA	0.1458	Risk	Mod-Strong		Anesthesia-reg.	Angiogenesis
EPHX2	-0.1198	Protective	Moderate		Lipid metab.	Epoxy hydrol.
CHRNA1	-0.1144	Protective	Not det.		nACh receptor	Muscle nAChR
GABRE	0.1080	Risk	Not det.		GABA receptor	epsilon GABA-A
KCNMA1	0.0966	Risk	Weak-Mod		K+ channel	BK K+ ch.
CDKN2A	0.0848	Risk	Weak-Mod	**Yes (COAD, P<0.001)**	Cell cycle	p16 CDK inh.
AQP1	0.0605	Risk	Mod-Strong		Fluid balance	Water channel
PHKG1	-0.0525	Protective	Weak		Glycogen metab.	Phos kinase
GLRB	0.0463	Risk	Not det.		Glycine receptor	Glycine beta
CACNA1C	0.0138	Risk	Not det.		Ca2+ channel	L-type Ca2+ ch.
ITPKB	0.0099	Risk	Moderate		Ca2+ signaling	IP3 kinase

Analysis Pipeline: TCGA-CRC (n=623 tumor) -> DEARG (78 genes) -> LASSO Cox (15-gene model) -> External Evaluation (GSE17536, GSE39582) -> Clinical Analysis (Cox, Nomogram, ROC, DCA) -> GO/KEGG Enrichment -> GSEA -> Immune Infiltration -> TIDE + TCIA IPS -> Drug Sensitivity -> Cell Type Association

Figure 5

Cell-type association and model summary. (A) Spearman correlation heatmap between 15 model genes and ssGSEA-based 22 immune-cell scores (asterisks indicate FDR < 0.05). (B) Expression differences of model genes across immune-infiltration strata. (C) Summary table of the 15-gene model including coefficients, risk direction, HPA IHC status, and functional category.

Supplementary Files

This is a list of supplementary files associated with this preprint. Click to download.

- TRIPODChecklist.docx
- SupplementaryInformation.pdf
- SupplementaryInformationsource.docx